

Application of Nonlinear Estimation Strategies on a Magnetorheological Suspension System with Skyhook Control

Andrew S. Lee
Mechanical Engineering
University of Guelph
Guelph, Ontario, Canada
alee32@uoguelph.ca

S. Andrew Gadsden
Mechanical Engineering
University of Guelph
Guelph, Ontario, Canada
gadsden@uoguelph.ca

Mohammad Al-Shabi
Mechanical Engineering
University of Sharjah
Sharjah, UAE
malshabi@sharjah.ac.ae

Abstract—Extraction of state values from noisy or uncertain systems is important for feedback control because it improves the accuracy of the error signal. For known linear systems with Gaussian white noise, the Kalman filter provides optimal state estimates in terms of state error. However, electromechanical systems, such as magnetorheological dampers, typically exhibit nonlinear behaviour. In this paper, a new nonlinear estimation method known as the extended sliding innovation filter is presented and applied on a magnetorheological suspension system. The state estimates are extracted from a quarter car model with an active magnetorheological suspension system with skyhook control. The results are compared with the popular extended Kalman filter, and future experiments are considered.

Keywords—estimation theory, actuator, control

I. INTRODUCTION

The objective of estimation theory is to extract information on states in the presence of system and measurement noise. For known linear systems with Gaussian white noise, the Kalman filter (KF) produces the optimal state estimate [1]. The Kalman gain minimizes the trace of the updated state error covariance matrix and is proven to produce the optimal state estimate for known linear systems with Gaussian noise [1, 2, 3]. The KF has a wide range of applications, in areas such as target tracking, signal processing, and fault detection [4, 5, 6]. Similar to control theory, a trade-off exists between estimation accuracy and robustness to disturbances. Current research in estimation theory aims to reduce state estimation error while simultaneously being robust to disturbances, faults, and modeling uncertainty [1].

For nonlinear systems, several strategies have been proposed. The extended Kalman Filter (EKF) can be used to estimate the states of a nonlinear dynamic system. The filter uses local linearization of the system model at the operating point in order to calculate the corrective Kalman gain [1, 4]. The EKF derivation is based on the first-order Taylor series expansion of the nonlinear system model, also known as a Jacobian matrix [1]. However, if the system is highly nonlinear, the EKF solution may diverge from the true state trajectory leading to numerical instabilities and poor estimation results [7].

Another nonlinear estimation strategy is the sigma-point Kalman filter (SPKF), which is formulated using a weighted statistical linear regression approach that linearizes the nonlinear state model statistically [8]. The SPKF produces

sigma points from the projected probability distribution of states and are mapped through the nonlinear system model [8]. Unlike the EKF, this system does not require local linearization of the system model which improves the estimation process for nonlinear systems [4].

Similarly, the unscented Kalman filter (UKF) also uses sigma points from the projected probability distribution of states [8]. The UKF uses a deterministic sampling approach known as the unscented transform to select a minimal set of sample points around the mean [1, 4]. It is possible to approximately determine the mean and covariance of the density using Monte Carlo sampling [1]. The UKF can capture the updated statistical mean and covariance up to the third-order for any nonlinearity; making it superior to the EKF in terms of estimation accuracy [1, 7]. However, like many particle filters, the UKF is resource intensive and may suffer from poor sampling rates [4].

The smooth variable structure filter (SVSF) was introduced in an effort to improve upon the robustness of estimation strategies [9]. The derivation of the SVSF gain yields a switching function based on variable structure techniques [9]. The gain is a function of measurement error and a switching term that keeps the estimates along the true state trajectory [9]. Stability is improved by defining an upper bound on noise and modeling uncertainty which improves robustness to uncertainties and disturbances.

Most recently, a new filter was introduced based on variable structure techniques similar to the SVSF called the sliding innovation filter (SIF) [10]. The SIF is a robust estimation strategy that provides a stable estimation process, and has been found to be more accurate than the SVSF [10]. Similar to the SVSF, the SIF creates an upper bound on noise and modeling uncertainty but uses a different method for calculating the corrective gain term. In this paper, similar to the EKF, the SIF is extended to nonlinear systems, and is referred to as the extended sliding innovation filter (ESIF). The ESIF is compared with the popular EKF as a benchmark. The filters are applied to an electromechanical system consisting of a quarter car model with skyhook control using a magnetorheological (MR) damper for active damping.

The paper is organized as follows. In Section II, the background on magnetorheological systems is provided. The ESIF equations are provided in Section III. The simulation setup and results are discussed in Section IV, followed by concluding remarks.

II. MAGNETORHEOLOGICAL SYSTEMS

A. Magnetorheological Fluids

Magnetorheological fluids are a class of smart fluids that significantly change viscosity when a magnetic field is applied. The fluid consists of micron scale (1 to 10 μm) magnetically polarizable particles suspended in a carrier medium such as mineral or silicon oil [11]. Surfactants are often used in the non-colloidal mixture in order to prevent the settling of the suspended particles [12]. The magnetic particles typically account for 20 to 60 percent of the MR fluid's total volume [11]. The MR fluid reacts nearly instantaneously allowing for smooth force adjusting and repeatability [13].

When a magnetic field is applied to the MR fluid, the ferromagnetic particles rearrange to form linear structures and chains. The formation of these structures results in a change in the fluid's viscosity. Increasing the strength of the magnetic field increases the yield strength of the MR fluid [14]. Since the discovery of the MR fluid effect in the 1940s by Jacob Rabinov, commercial products have been developed to attain low viscosities and high yield stresses; a 100 kPa yield stress is achievable within a few milliseconds [14, 15].

This property has three main engineering application modes: flow (valve) mode, shear mode and squeeze mode [12]. In flow mode, the magnetic field is normal to the flow of the MR fluid and is typically used for linear dampers [12]. In shear mode, the magnetic field is normal to the displacement of the shear walls and is used for rotary dampers, breaks, and clutches [12]. Finally, squeeze mode utilizes a magnetic field that is parallel to the desired displacement of the containing walls. The squeeze mode provides large forces for relatively small displacements [12].

B. Magnetorheological Dampers

The quick response time of MR fluid behavior when exposed to a magnetic field is ideal for electromechanical devices such as actuators and dampers. Semi-active MR control devices have the versatility of active dampers while retaining the reliability of passive ones [12]. The two main engineering applications of MR fluids are linear and rotary dampers.

The main advantage of linear MR dampers is the controllability of the system damping by changing the input current. By changing the current, the magnetic induction in an orifice between two separated MR fluid chambers is regulated [12]. Linear MR dampers such as the one shown in Fig. 1 use the MR fluid in flow mode to treat the orifice as a valve for the MR fluid. One of the first applications of linear MR dampers in the automotive industry is its use as a secondary suspension element for on and off highway vehicles [15]. By controlling the damping arrangement, the excitation frequency and vibration transmission can be adjusted as desired [15].

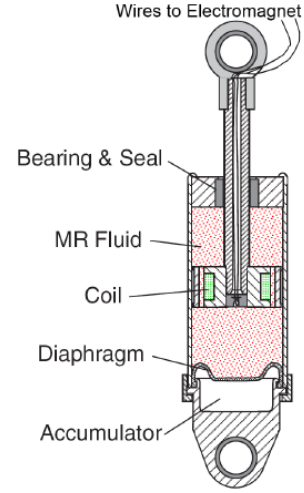


Figure 1. Schematic of a single ended linear MR damper [12].

C. Magnetorheological Force-Velocity Hysteresis Model

Several different models have been proposed in literature to describe the force-velocity hysteresis curve of linear MR dampers including bi-viscous, polynomial, Bouc-Wen, and Sigmoid [14, 15, 16]. While the Bouc-Wen produces the best estimates according to [16], the polynomial model produces reasonable estimates and was chosen due to ease of implementation for the EKF and proposed ESIF.

The force-velocity relationship of an MR damper is highly dependent on the applied current. The damping force f_d of the MR damper can be described by the following:

$$f_d = f_i(i)f_h(y, \dot{y}, \ddot{y}) \quad (2.1)$$

where f_i is a function of current i , and f_h describes the hysteretic behavior of the piston displacement, velocity, and acceleration denoted by y , \dot{y} , and \ddot{y} , respectively [16]. The nonlinear incremental current proposed by [16] is as follows:

$$f_i(i) = 1 + \frac{k_i}{1 + e^{-a(i+I_0)}} - \frac{k_i}{1 + e^{-aI_0}}; \quad i \geq 0 \quad (2.2)$$

where k , a , and I_0 are constants obtained through measured data. A model of the piecewise polynomial function to describe the MR damper during positive and negative acceleration was first proposed by [17]. The polynomial hysteresis function is as follows:

$$f_h = \left(\sum_{k=0}^n b_k \dot{y}(t)^k \right); \quad n = 6 \quad (2.3)$$

where b_k represents the polynomial coefficient constants obtained through experimentation, k is the polynomial exponent, and n is the order of the polynomial. By combining (2.2) and (2.3) the damping force function becomes:

$$f_d = \begin{cases} f_i(i) \left(\sum_{k=0}^6 b_{uk} \dot{y}(t)^k \right); & \dot{x} < 0 \\ f_i(i) \left(\sum_{k=0}^6 b_{dk} \dot{y}(t)^k \right); & \dot{x} > 0 \\ f_i(i) \left(\sum_{k=0}^6 \frac{1}{2} (b_{uk} + b_{dk}) \dot{y}(t)^k \right); & \dot{x} = 0 \end{cases} \quad (2.4)$$

where b_{uk} and b_{dk} represent the coefficients of the upper and lower polynomial, respectively [16]. In order to ensure the convergence of the two polynomial functions near the extremities, when the piston acceleration is zero, the damping force is calculated as the average of the upper and lower polynomial functions [16]. The value of the constants and polynomial coefficients used in this paper can be found in the Appendix.

III. THE EXTENDED SLIDING INNOVATION FILTER

In this paper, a nonlinear form of the SIF is presented referred to as the extended sliding innovation filter (ESIF). Similar to the extended Kalman filter (EKF), the proposed ESIF makes use of the linearized form of the nonlinear system and measurement functions [4]. For example, consider the nonlinear system function $f(\hat{x}_{k|k}, u_k)$ and the nonlinear measurement function $h(\hat{x}_{k+1|k})$. Linearized forms of these nonlinearities may be calculated using the following partial derivatives (Jacobians), respectively:

$$F_{k+1} = \left. \frac{\partial f}{\partial x} \right|_{\hat{x}_{k|k}, u_k} \quad (3.1)$$

$$H_{k+1} = \left. \frac{\partial h}{\partial x} \right|_{\hat{x}_{k+1|k}} \quad (3.2)$$

where x refers to the state, \hat{x} refers to the state estimate, u refers to the control signal input, k refers to the time step, $k+1|k$ refers to the prediction step, and $k|k$ refers to the previous time update step. The structure of the nonlinear SIF estimation process is similar to the EKF with the main difference being the formulation of the gain. The SIF and ESIF are both predictor-corrector estimators. The prediction stage consists of three main equations, as follows:

$$\hat{x}_{k+1|k} = f(\hat{x}_{k|k}, u_k) \quad (3.3)$$

$$P_{k+1|k} = F_{k+1}P_{k|k}F_{k+1}^T + Q_{k+1} \quad (3.4)$$

$$\tilde{z}_{k+1|k} = z_{k+1} - h(\hat{x}_{k+1|k}) \quad (3.5)$$

Note that f refers to the nonlinear system function, F_k refers to the linearized version of the system matrix A (Jacobian matrix or first-order Taylor series expansion) at time k , and h refers to the nonlinear measurement function. The states are first predicted in (3.3) before being updated in (3.7) using the gain defined in (3.6). The state error covariance matrix is first predicted in (3.4) before being updated in (3.8). Note that the gain (3.6) is also used to update the state error covariance (3.8). The update stage consists of three main equations, as follows:

$$K_{k+1} = H_{k+1}^+ \overline{\text{sat}}(|\tilde{z}_{k+1|k}|/\delta) \quad (3.6)$$

$$\hat{x}_{k+1|k+1} = \hat{x}_{k+1|k} + K_{k+1}\tilde{z}_{k+1|k} \quad (3.7)$$

$$P_{k+1|k+1} = (I - K_{k+1}H_{k+1})P_{k+1|k}(I - K_{k+1}H_{k+1})^T \dots \\ \dots + K_{k+1}R_{k+1}K_{k+1}^T \quad (3.8)$$

Note that H_{k+1}^+ refers to the pseudoinverse of the linearized measurement matrix (first-order Taylor series expansion) at time k , $\overline{\text{sat}}$ refers to the diagonal of the saturation term, sat refers to the saturation of a value (yields a result between -1

and +1), $|\tilde{z}_{k+1|k}|$ refers to the absolute value of the innovation, δ refers to the sliding boundary layer, I refers to the identity matrix (of dimension n -by- n where n is the number of states), R refers to the measurement noise covariance, and $k+1|k+1$ refers to the updated values at time $k+1$ based on information at time $k+1$. Equations (3.1) through (3.8) represent the proposed ESIF estimation process for nonlinear systems and measurements.

IV. COMPUTER SIMULATIONS AND RESULTS

A. Quarter Car Model with Active Damper

The EKF and ESIF were applied to a quarter car model based on Fig. 2. The equations of motion are defined as follows:

$$M_s \ddot{x}_1 + k_s(x_1 - x_3) + f_d = 0 \quad (4.1)$$

$$M_u \ddot{x}_3 + k_s(x_3 - x_1) + k_t(x_3 - r) + \dots \\ \dots b_s(\dot{x}_3 - \dot{x}_1) + b_t(\dot{x}_3 - \dot{r}) + f_d = 0 \quad (4.2)$$

where M_s and M_u are the sprung mass and unsprung mass, respectively, k_s and b_s are the spring constant and damping coefficient between the sprung mass and the unsprung mass, respectively, k_t and b_t are the spring constant and damping coefficient of the tire, respectively, and r is the road profile (defined later in Fig. 3). As stated previously, f_d is the damping force exerted by the MR damper. The state space equations based on this model and used in the simulation are defined as follows:

$$\dot{x}_1 = x_2 \quad (4.3)$$

$$\dot{x}_2 = (k_s(x_3 - x_1) - f_d)/M_s \quad (4.4)$$

$$\dot{x}_3 = x_4 \quad (4.5)$$

$$\dot{x}_4 = (k_s(x_1 - x_3) + k_t(x_1 - r_3) + \dots \\ \dots b_s(x_2 - x_4) + b_t(\dot{r} - \dot{x}_4) - f_d)/M_u \quad (4.6)$$

The value of the constants used in the simulation are available in the Appendix. The skyhook criterion used to control the MR damper is described as follows:

$$x_2(x_2 - x_4) \geq 0; \quad i = 1 \text{ amp} \\ x_2(x_2 - x_4) = 0; \quad i = 0 \text{ amp} \quad (4.7)$$

If the relative velocity of the sprung mass with respect to the unsprung mass is in the same direction as the velocity of the unsprung mass, then a current is applied to the MR damper in order to reduce the body acceleration [18]. For this controller, estimation of the velocities states of each mass is crucial in order to make sure the system meets the skyhook criterion for MR damper activation.

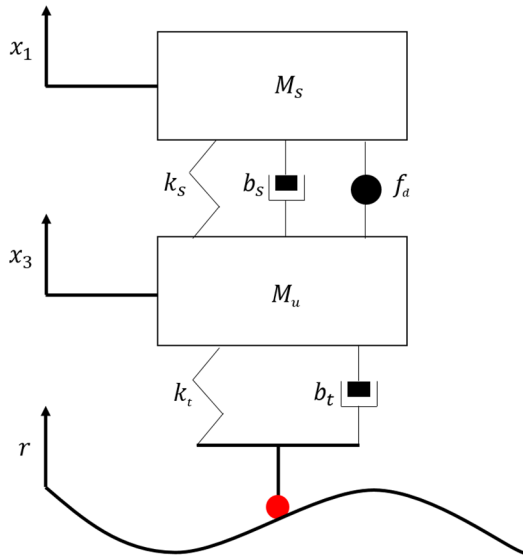


Figure 2. Quarter car model used in simulation to compare EKF and ESIF.

The EKF and ESIF methods were investigated using Matlab to simulate the quarter car model, implement a skyhook controller, and generate a road profile. The simulation used a flat road profile with a bump encountered at four seconds (a disturbance) and a sample rate of 1 ms. The bump was simulated using a sinusoid with an amplitude of 5 cm and frequency of 0.5 Hz as shown in Fig 3.

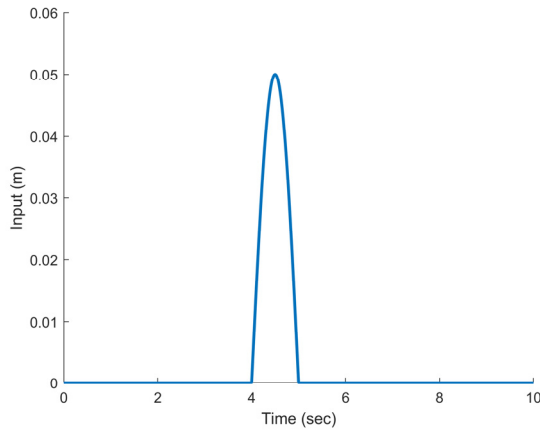


Figure 3. Road profile (with a disturbance) used in simulation.

The quarter car model was first tested without the activation of the skyhook controller and MR damper in order to visualize the free dynamics of the system. The position of the sprung mass is shown in Fig. 4. Note that the system and measurement noise covariances used in the simulation were defined as Q and R , respectively:

$$Q = \text{diag}[10^{-9} \quad 10^{-8} \quad 10^{-9} \quad 10^{-8}] \quad (4.8)$$

$$R = \text{diag}[10^{-5} \quad 10^{-4} \quad 10^{-5} \quad 10^{-4}] \quad (4.9)$$

The EKF and SIF have similar performances when predicting the states when no controller or MR damper is applied. This is because without the use of the MR damper, the quarter car system is linear and uses Gaussian white noise to

describe the system and measure noise. In this scenario, the EKF should provide similar performance to the ESIF.

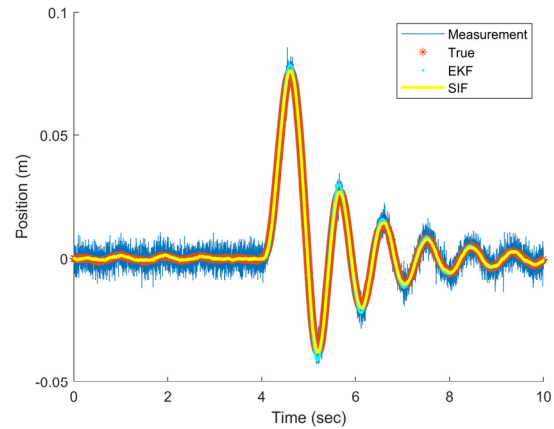


Figure 4. Sprung mass position without skyhook controller.

The skyhook controller was implanted by using velocities state estimates from the EKF and ESIF as feedback. The sliding boundary layer widths used for the ESIF were tuned manually based on reducing estimation error, and defined as:

$$\delta = \text{diag}([0.5 \quad 1 \quad 0.5 \quad 0.09]) \quad (4.10)$$

The position of the sprung mass using the EKF and ESIF in the skyhook controller is shown in Fig. 5.

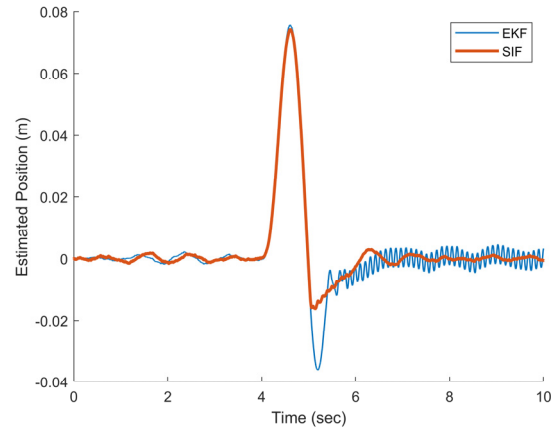


Figure 5. Skyhook controller performance using EKF and ESIF.

Both filters perform comparatively before the MR damper and skyhook controller is activated (at approximately five seconds) because the road profile is flat and the system dynamics remain relatively linear before the MR damper is activated. The initial bumps are a result of system noise.

When the skyhook controller is activated, the system dynamics become highly nonlinear due to the piecewise 6th-order polynomial force-velocity hysteresis model of the MR damper. This results in poor velocity state estimates for the EKF. The local linearization of the system cannot accurately model the system. The poor velocity state estimates result in erratic behavior of the skyhook controller as seen by the chattering in Fig. 5. The velocity estimates of the EKF can be seen in Fig. 6. The EKF reports higher velocities than the true values and does not capture the magnitude of the oscillations.

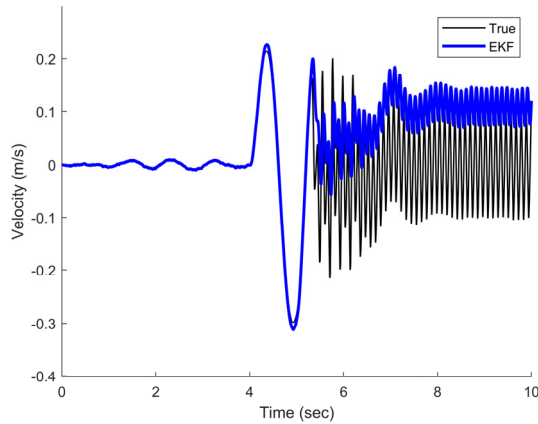


Figure 6. EKF sprung mass velocity estimates.

In order to fairly compare the EKF with the ESIF, the accuracy of both filters was assessed using the same controller input for the predicted state estimate. The result of the simulation is shown in Fig. 7. During the initial activation of the MR damper, the EKF deviates from the true state value as seen at five seconds. The EKF is able to converge as the amplitude of the sprung mass oscillation decreases, however it does so more slowly when compared with the ESIF.

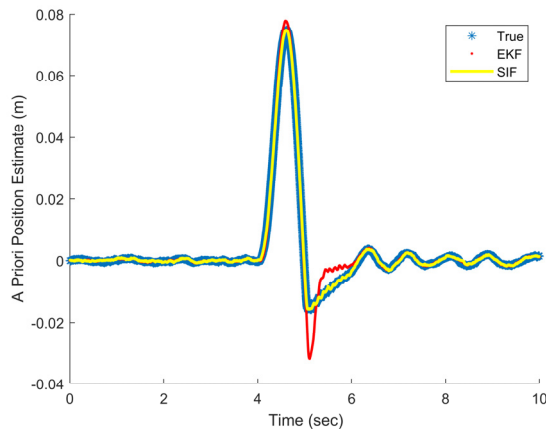


Figure 7. Comparison of predicted state estimates for EKF and ESIF.

The normalized error squared (NES) was plotted for both filters and is shown in Fig. 8. The EKF estimates can be shown to deviate from the true states when the MR damper is activated as shown by the sharp error spikes around four seconds, while the ESIF estimates follow the true states relatively closely throughout the entire simulation. This further highlights the robustness of the ESIF due to the switching function of the gain.

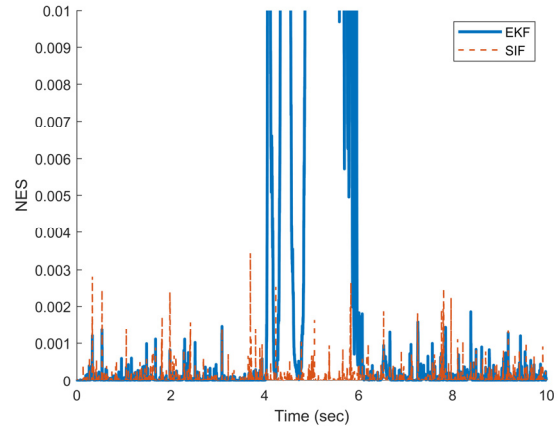


Figure 8. Normalized error squared (truncated at 0.01).

As shown in Table I, the root mean square error (RMSE) was calculated for each filter [4]. The ESIF was found to outperform the EKF, especially in terms of velocity state estimation, which is a crucial component of the skyhook controller.

TABLE I. RMSE VALUES

Filter	State			
	<i>Sprung Mass Position (m)</i>	<i>Sprung Mass Velocity (m/s)</i>	<i>Unsprung Mass Position (m)</i>	<i>Unsprung Mass Velocity (m/s)</i>
EKF	0.0023	0.0154	0.0008	0.0121
ESIF	0.0003	0.0013	0.0002	0.0043

V. CONCLUSIONS

While extracting state values from linear systems using model-based filters is relatively simple to implement, estimating states from nonlinear systems are far more challenging. Highly nonlinear systems such as MR dampers require novel approaches to achieve robust and accurate estimation. This paper presented a novel nonlinear estimation filter called the extended sliding innovation filter (ESIF). The ESIF uses a sliding boundary layer to represent the upper bounds of noise and modeling uncertainty. Using this approach, the ESIF was able to outperform the EKF which is known to have difficulties with highly nonlinear systems and uncertainties. The ESIF improved performance of the skyhook controller which was highly dependent on the accuracy of the velocity state estimates of the system.

APPENDIX

In this section, the parameters used in the simulation for the hysteresis and quarter car models are provided.

TABLE II. PARAMETERS FOR HYSTERESIS MODEL

Parameter	Value
k_t	3.10
a	18.53
I_0	-0.15
b_{u0}	0.06
b_{u1}	4.97
b_{u2}	-71.29
b_{u3}	-1,461.82
b_{u4}	23,232.45
b_{u5}	190,972.68
b_{u6}	-2,319,223.80
b_{d0}	-0.07
b_{d1}	5.03
b_{d2}	78.00
b_{d3}	-1549.09
b_{d4}	-27,398.44
b_{d5}	210,738.82
b_{d6}	3,017,864.40

TABLE III. PARAMETERS FOR QUARTER CAR MODEL

Parameter	Value
M_s	290 Kg
M_u	59 Kg
k_s	14,500 N/m
b_s	1,385.4 N · s/m
k_t	19,000 N/m
b_t	170 N · s/m

REFERENCES

- [1] H. H. Afshari, S. A. Gadsden and S. R. Habibi, "Gaussian Filters for Parameter and State Estimation: A General Review and Recent Trends," *Signal Processing*, vol. 135, pp. 218-238, 2017.
- [2] B. Ristic, S. Arulampalam and N. Gordon, *Beyond the Kalman Filter: Particle Filters for Tracking Applications*, Boston: Artech House, 2004.
- [3] S. Haykin, *Kalman Filtering and Neural Networks*, New York: John Wiley and Sons, Inc., 2001.
- [4] S. A. Gadsden, "Smooth Variable Structure Filtering: Theory and Applications," McMaster University, Hamilton, 2011.
- [5] S. A. Gadsden, M. Al-Shabi and S. R. Habibi, "Estimation Strategies for the Condition Monitoring of a Battery System in a Hybrid Electric Vehicle," *ISRN Signal Processing*, 2011.
- [6] S. A. Gadsden, Y. Song and S. R. Habibi, "Novel Model-Based Estimators for the Purposes of Fault Detection and Diagnosis,"

- IEEE/ASME Transactions on Mechatronics*, vol. 18, no. 4, pp. 1237-1249, 2013.
- [7] S. A. Gadsden, S. R. Habibi and T. Kirubarajan, "Kalman and Smooth Variable Structure Filters for Robust Estimation," *IEEE Transactions on Aerospace and Electronic Systems*, vol. 50, no. 2, pp. 1038-1050, 2014.
- [8] S. J. Julier and J. K. Uhlmann, "Unscented Filtering and Nonlinear Estimation," *Proceedings of the IEEE*, vol. 92, no. 3, 2004.
- [9] S. R. Habibi, "The Smooth Variable Structure Filter," *Proceedings of IEEE*, vol. 95, no. 5, pp. 1026-1059, 2007.
- [10] S. A. Gadsden and M. Al-Shabi, "The Sliding Innovation Filter," *IEEE Access*, vol. 8, pp. 96129-96138, 2020.
- [11] A. Milecki, "Investigation and Control of Magneto-Rheological Fluid Dampers," *International Journal of Machine Tools and Manufacture*, vol. 41, no. 3, pp. 379-391, 2001.
- [12] A. Spaggiari, "Properties and Applications of Magnetorheological Fluids," *Frattura ed Integrità Strutturale*, vol. 23, no. 23, pp. 57-61, 2013.
- [13] D. Guth and J. Mas, "Energy-Efficient Clutch with Optimized Torque Density," in *Smart Materials, Adaptive Structures and Intelligent Systems*, Snowbird, Utah, 2013.
- [14] P. Yadmellat and M. R. Kermani, "Adaptive Hysteresis Compensation for a Magneto-Rheological Robot," in *IEEE Intelligent Robots and Systems (IROS)*, Tokyo, Japan, 2013.
- [15] A. Olabi and A. Grunwald, "Design and Application of Magneto-Rheological Fluid," *Materials and Design*, vol. 28, no. 10, pp. 2658-2664, 2007.
- [16] X. Q. Ma, S. Rakesha and C. Su, "Development and Relative Assessments of Models for Characterizing the Current Dependent Hysteresis Properties of Magnetorheological Fluid Dampers," *Journal of Intelligent Material Systems and Structures*, vol. 18, pp. 487-502, 2007.
- [17] S. B. Choi, B. K. Lee and Y. P. Park, "A Hysteresis Model for the Field-dependent Damping Force of a Magnetorheological Damper," *Journal of Sound and Vibration*, vol. 2, no. 245, p. 375, 2001.
- [18] H. Sleiman, B. Lemaire-Semail, B. Clenet and J. Lozada, "Modeling and Inversion-based Control of a Magnetorheological Vehicle Suspension," in *IEEE Vehicle Power and Propulsion Conference*, Lille, France, 2010.